Check for updates

View Article Online
View Journal

Materials Horizons

Accepted Manuscript

This article can be cited before page numbers have been issued, to do this please use: S. S. Jana and T. Maiti, *Mater. Horiz.*, 2023, DOI: 10.1039/D2MH01488B.

This is an Accepted Manuscript, which has been through the Royal Society of Chemistry peer review process and has been accepted for publication.

Accepted Manuscripts are published online shortly after acceptance, before technical editing, formatting and proof reading. Using this free service, authors can make their results available to the community, in citable form, before we publish the edited article. We will replace this Accepted Manuscript with the edited and formatted Advance Article as soon as it is available.

You can find more information about Accepted Manuscripts in the Information for Authors.

Please note that technical editing may introduce minor changes to the text and/or graphics, which may alter content. The journal's standard Terms & Conditions and the Ethical guidelines still apply. In no event shall the Royal Society of Chemistry be held responsible for any errors or omissions in this Accepted Manuscript or any consequences arising from the use of any information it contains.

ROYAL SOCIETY OF CHEMISTRY

rsc.li/materials-horizons

View Article Online
DOI: 10.1039/D2MH01488B

New concepts

This work demonstrates an exciting approach to design a thermoelectric material utilizing high entropy effect. For the first time, we have designed a novel tungsten bronze structure type high entropy oxide for the thermoelectric applications. We have determined the phase stability of the *HETB* by using thermodynamic calculation. Led by multi-phonon scattering due to presence of 5 cations in HETB, we have been able to reach ultralow thermal conductivity, which is the lowest ever reported value in rare-earth-free high entropy oxide thermoelectrics. Besides, large Seebeck coefficient has been obtained due to the presence of multivalent cations. Increased Seebeck coefficient and ultralow thermal conductivity synergistically allow *HETB* to attain maximum *ZT* performance among rare-earth-free high entropy oxide thermoelectrics. Our strategy of designing rare earth free high entropy niobate with tungsten bronze structure opens up a new avenue for developing low-cost oxide thermoelectric materials.

Published on 28 February 2023. Downloaded by Indian Institute of Technology Kanpur on 3/7/2023 11:08:22 AM.

Materials Horizons Accepted Manuscript

View Article Online
DOI: 10.1039/D2MH01488B

Designing Rare Earth Free High Entropy Oxide with Tungsten Bronze Structure for Thermoelectric Application

*Subhra Sourav Jana and Tanmoy Maiti**

Plasmonics and Perovskites Laboratory, Department of Materials Science and Engineering, IIT Kanpur, U.P. 208016, India.

Published on 28 February 2023. Downloaded by Indian Institute of Technology Kanpur on 3/7/2023 11:08:22 AM.

Materials Horizons Accepted Manuscript

Abstract:

In recent years, forming high entropy oxides has emerged as one of the promising approaches to designing oxide thermoelectrics. Entropy engineering is an excellent strategy to improve thermoelectric performance by minimizing the thermal conductivity arising from enhanced multi-phonon scattering. In the present work, we have successfully synthesized rare-earth-free single phase solid solution of novel high entropy niobate $(Sr_{0.2}Ba_{0.2}Li_{0.2}K_{0.2}Na_{0.2})Nb_2O_6$, with tungsten bronze structure. This is the first report on the thermoelectric properties of high entropy tungsten bronze type structures. We have obtained maximum Seebeck coefficient of $-370\mu VK^{-1}$ at $1150K$, which is the highest among tungsten bronze type oxide thermoelectrics. The minimum thermal conductivity of $0.8\ Wm^{-1}K^{-1}$ is obtained at $330K$, which is so far the lowest reported value among rare-earth-free high entropy oxide thermoelectrics. This synergistic combination of large Seebeck and record low thermal conductivity gives rise to a maximum ZT of 0.23 which is so far the highest among rare-earth free high entropy oxide-based thermoelectrics.

* Corresponding author Telephone: +91-512-259-6599; Email address: tmaiti@iitk.ac.in

View Article Online
DOI: 10.1039/D2MH01488B

Published on 28 February 2023. Downloaded by Indian Institute of Technology Kanpur on 3/7/2023 11:08:22 AM.

Materials Horizons Accepted Manuscript

Introduction:

In response to the global energy crisis, thermoelectric power generator (TEG) has emerged as one of the most important research areas in the field of material science. TEG has the ability to convert waste heat directly into useful electricity without much carbon footprint. The conversion efficiency of a thermoelectric material is related to the dimensionless figure of merit, ZT ($= \frac{S^2\sigma}{\kappa} T$), where S denotes the Seebeck coefficient, σ is electrical conductivity, and κ is thermal conductivity. Oxide-based thermoelectrics[1] offer enormous potential for high temperature waste heat recovery over the state-of-the-art Chalcogenides owing to their certain advantages, such as environmental friendliness, low-cost processing, high temperature stability. However, they suffer from poor thermoelectric performance (low ZT) due to several drawbacks, one of which is high thermal conductivity.[2] Nano structuring has been considered as one of the well-known successful strategies to reduce the thermal conductivity in chalcogenides and intermetallics. However, the very same strategy could not be effective for oxides, since the oxides inherently possess the phonon mean free path in the nanoscale range. This warrants a new strategy to design a novel thermoelectric material, possessing a lower phonon mean free path ($< 1nm$). Recently, Banerjee *et al.*[3] have shown that the formation of the high entropy perovskite, $Sr(Ti_{0.2}Fe_{0.2}Mo_{0.2}Nb_{0.2}Cr_{0.2})O_3$ can help in achieving a lower mean free path, which gives rise to attain ultralow thermal conductivity. The concept of high entropy effect has been translated into oxides by Rost *et al.*[4], when they have reported a single phase rock salt structure $(Mg_{0.2}Zn_{0.2}Co_{0.2}Cu_{0.2}Zn_{0.2})O$ by mixing 5 component oxides. High entropy effect is expected to have a remarkable importance on improving thermoelectric properties. Disorder atomic arrangements along with variations in atomic mass in high entropy oxides offer increasing phonon scattering, thereby suppressing lattice thermal conductivity. On the other hand, high configurational entropy can also cause the enhancement in crystal symmetry

View Article Online
DOI: 10.1039/D2MH01488B

Published on 28 February 2023. Downloaded by Indian Institute of Technology Kanpur on 3/7/2023 11:08:22 AM.

and hence, the degree of band degeneracy, which can further increase the Seebeck coefficient.[7] Therefore, entropy optimization can be a viable approach towards synergistically attaining the goal of improved electrical transport and lower lattice thermal conductivity. Very recently, a few other thermoelectric oxides have also been developed using the concept of high entropy effect.[8–10] They exhibit quite a large Seebeck coefficient, but their thermal conductivity is almost more than twice than that of $Sr(Ti_{0.2}Fe_{0.2}Mo_{0.2}Nb_{0.2}Cr_{0.2})O_3$. Moreover, they consist of rare earth elements like Ce, La[8–10] and toxic elements like Pb,[10] which further serve as drawbacks.

Although few high entropy oxides with perovskite structure have been investigated, no other high entropy oxides with different crystal symmetry have been reported till date for thermoelectric applications. The current work focuses on the development of a novel high entropy oxide with a tungsten bronze structure for high temperature thermoelectric applications. $Sr_xBa_{1-x}Nb_2O_6$ (SBN), a well-known traditional ferroelectric material with tungsten bronze structure, has become a new viable option in the group of n-type oxide thermoelectrics, since Lee *et al.*[11] reported excellent power factor ($2000\ \mu W m^{-1}K^{-2}$ at $516K$) in the direction parallel to c axis of single crystal SBN. However, polycrystalline SBN shows poor *ZT* performance (~ 0.2 at $1073\ K$)[12] in comparison to other n-type oxide thermoelectrics such as ZnO (0.65 at $1247K$),[13] $SrTiO_3$(0.6 at $1100K$).[14] The Seebeck coefficient of polycrystalline SBN is much lower (~ 2 times)than that of single crystal SBN,[11] even when doped with various rare earth oxides.[12,15–17] Moreover, the thermal conductivity of SBN doesn't get lowered in ceramic form compared with its single crystal counterpart. Therefore, high entropy approach on SBN based oxide by populating A site can offer a tremendous possibility in supressing thermal conductivity and increasing Seebeck coefficient at the same time.

In the present work, a rare-earth-free high entropy oxide with a nominal composition of $(Sr_{0.2}Ba_{0.2}Li_{0.2}K_{0.2}Na_{0.2})Nb_2O_6$ (*HETB*), possessing a tungsten bronze crystal structure, has

Materials Horizons Accepted Manuscript

View Article Online
DOI: 10.1039/D2MH01488B

been explored for the first time for thermoelectric application. We have obtained a remarkable Seebeck coefficient of $-370\mu VK^{-1}$ at $1150K$, which is so far the highest among SBN based tungsten bronze oxides. Further, electron transport has been explained using the small polaron hopping model. Moreover, we have been able to reach the minimum lattice thermal conductivity of $0.8Wm^{-1}K^{-1}$ near $470K$, which is close to their theoretical limit, as estimated by Cahil's formula.[18]

Thermodynamic calculation:

A novel high entropy oxide, having a nominal composition of $(Sr_{0.2}Ba_{0.2}Li_{0.2}K_{0.2}Na_{0.2})Nb_2O_6$ with a tetragonal tungsten bronze structure, has been fabricated, where $SrCO_3$, $BaCO_3$, Li_2CO_3, Na_2CO_3, K_2CO_3, and Nb_2O_5 have been used as precursor oxides. Simple SBN based tungsten bronze structure itself is a complex crystal structure, composed of NbO_6 octahedron framework in which the octahedrons share their corners, resulting in the formation of pentagonal (A1), tetragonal (A2), and trigonal (C) interstitial sites.[19–21] Sr, Na, K, Li and Ba are distributed among the A1 and A2 sites. Generally, C site remains vacant in tungsten bronze structure due to its small trigonal interstitial size. However, small amount of Li is expected to go in the trigonal interstitial void due to its smaller size. But that is not accounted for in our calculation for the sake of simplicity. Further, all the interstitial sites here are surrounded by identical NbO_6 octahedrons, these A1 and A2 sites are presumed to be identical, commonly referred to as the A site.

The change of enthalpy ($\Delta H_{thermal}$) and entropy ($\Delta S_{thermal}$) are given by the equations (1&2)

$$\Delta H_{thermal} = H_t^0 - H_{298}^0 = At + \frac{Bt^2}{2} + \frac{Ct^3}{3} + \frac{Dt^4}{4} - \frac{E}{t} + F - H_f \ldots\ldots(1)$$

$$\Delta S_{thermal} = Alnt + Bt + \frac{Ct^2}{2} + \frac{Dt^3}{3} - \frac{E}{2t^2} + G \ldots(2)$$

Published on 28 February 2023. Downloaded by Indian Institute of Technology Kanpur on 3/7/2023 11:08:22 AM.

Materials Horizons Accepted Manuscript

View Article Online
DOI: 10.1039/D2MH01488B

Published on 28 February 2023. Downloaded by Indian Institute of Technology Kanpur on 3/7/2023 11:08:22 AM.

Where, A, B, C, D, E, F, G are substance dependent constants and 't' is temperature in K. $\frac{H_f}{1000}$ is enthalpy of formation of an oxide (say $A_aB_bO_y$) that is expressed by modified Pauling's formula, as proposed by Aronson in equation (3).[22]

$$H_f = -96.5 \times y[n_A(\chi_A - \chi_O)^2 + n_B(\chi_B - \chi_O)^2] + 108.8y \ldots.(3)$$

Where, χ and n are the electronegativity and molar fraction of different atoms, respectively. By putting the values of χ, n and y in equation (3), the formation enthalpy (H_f) of $-1443KJ.mol^{-1}$ has been computed for $(Sr_{0.2}Ba_{0.2}Li_{0.2}K_{0.2}Na_{0.2})Nb_2O_6$ at $1473K$. A, B, C, D, E all the parameters of the *HETB* have been estimated from fitting C_p data (**fig.S1**), using the equation (4).

$$C_p = A + B.T + C.T^2 + D.T^3 + \frac{E}{T^2} \ldots..(4)$$

F, G have been later calculated from the entropy calculation in equation (2). All the parameters are tabulated in **table S1**. Considering $H^0_{298} = 0$ and S = 0 at 0K as boundary conditions and plugging in all the constants in equation (1 & 2) $\Delta H_{thermal}$ and $\Delta S_{thermal}$ of *HETB* has been estimated as $-116KJ.mol^{-1}$and $-72KJ.mol^{-1}$, respectively. Hence, the free energy change of thermodynamic part ($\Delta G_{thermal}$) is calculated using the equation (5).

$$\Delta G_{thermal} = \Delta H_{thermal} - T\Delta S_{thermal} \ldots.(5)$$

$$= -10KJ.mol^{-1}$$

Finally, ΔG_{mix} has been determined from the equation (6).

$$\Delta G_{mix} = \Delta H_{mix} - T\Delta S_{mix} \ldots.(6)$$

ΔH_{mix} and ΔS_{mix} are change in mixing enthalpy and mixing entropy, respectively. K, Li, Na, Ba, Sr all are populated in the A site or the different sites formed by Nb-O octahedrons. Therefore, ΔH_{mix} has been assumed to have come from the A site only. ΔH_{mix} has been calculated using the equation (7), proposed by Midemma.[23]

Materials Horizons Accepted Manuscript

View Article Online
DOI: 10.1039/D2MH01488B

$$\Delta H_{mix} = \sum_{i=1, i \neq j}^{n} \Omega_{ij} X_i X_j$$

$$= \sum_{i=1, i \neq j}^{n} 4\Delta H_{AB}^{mix} . X_i X_j \ldots\ldots\ldots\ldots\ldots..(7)$$

Here, Ω_{ij} is the regular melt-interaction parameter, can be replaced by $4\Delta H_{AB}^{mix}$. $\Delta H_{AB}^{mix}$is mixing enthalpy of binary alloys listed in **table S2**, where A and B indicates all possible combination of elements. X_i and X_j are the concentration of i-th and j-th elements in a binary alloy compound. Entropy of mixing or often depicted as configuration entropy can be expressed in the equation (8)

$$\Delta S_{mix} = -R. \sum_{i=1, i \neq j}^{n} X_i . lnX_i \ldots\ldots\ldots\ldots\ldots\ldots..(8)$$

The ΔG_{mix} has been calculated to be $-15 KJ.mol^{-1}$ and finally ΔG_{total} is calculated.

$$\Delta G_{Total} = \Delta G_{Thermo} + \Delta G_{mix} \ldots\ldots\ldots(9)$$

$$= -10 KJ.mol^{-1} - 15 KJ.mol^{-1}$$

$$= -35 KJ.mol^{-1}$$

Overall negative ΔG_{Total} suggests that it is feasible to form the *HETB* single phase structure from precursor oxides. The calculated values of enthalpy, entropy and free energy are listed in **table 1**.

Table 1: Thermodynamic calculation date at $1473K$.

Composition	$\Delta H_{thermal}$ $(KJ.mol^{-1})$	$\Delta S_{thermal}$ $(KJ.mol^{-1})$	ΔH_{mix} $(KJ.mol^{-1})$	ΔS_{mix} $(J.mol^{-1})$	ΔG_{Total} $(KJ.mol^{-1})$
HETB	-116	-72	3.88	13	-35

Results and Discussions:

Phase and microstructure:

Published on 28 February 2023. Downloaded by Indian Institute of Technology Kanpur on 3/7/2023 11:08:22 AM.

Materials Horizons Accepted Manuscript

View Article Online
DOI: 10.1039/D2TH01488B

HETB has been synthesized using a solid state processing technique. Details of the processing have been illustrated in SI. X-ray diffraction (XRD) pattern in **fig.1(a)** shows the formation of single phase of *HETB*. No other secondary phase has been detected, as confirmed by the XRD pattern, which corroborates well with the preceding thermodynamic calculation. All the lattice planes of *HETB* have been indexed to a tetragonal crystal structure with the *P4bm* space group. Rietveld refinement of the powder XRD pattern has been performed as shown in **fig.1(b)** to estimate the lattice parameters. Considerably low values of fitting parameters, as given in **table S3**, indicate that the fitting is excellent. The fitted XRD profile reveals the lattice parameters to be $a = b = 12.48$Å and $c = 3.95$Å. All the atoms at A sites (Sr, Ba, Li, K, Na) are subjected to randomly occupy the interstitial voids, generated by NbO_6 octahedra, as schematically depicted in **fig.1(c)**. The FESEM image of the fractured surface in **fig.1(d)** reveals the *HETB* to possess larger grains with the dense microstructure. The Relative bulk density of the *HETB* pellets has been measured to be more than 95%, which corroborates well with the FESEM image.

Published on 28 February 2023. Downloaded by Indian Institute of Technology Kanpur on 3/7/2023 11:08:22 AM.

Materials Horizons Accepted Manuscript

View Article Online
DOI: 10.1039/D2MH01488B

Published on 28 February 2023. Downloaded by Indian Institute of Technology Kanpur on 3/7/2023 11:08:22 AM.

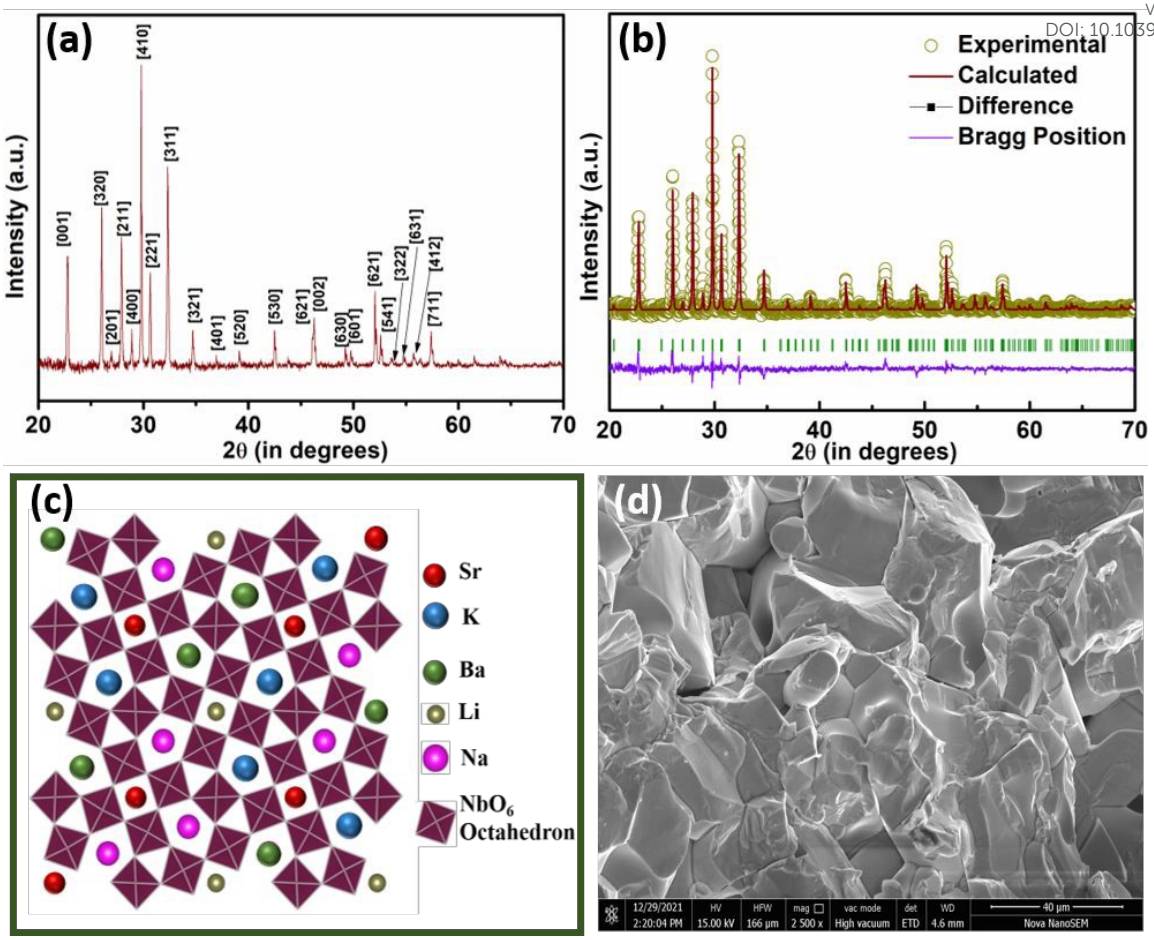

Fig.1 (a) Powder XRD pattern (b) rietveld refinement of XRD pattern (c) Schematics of *HETB* and (d) FESEM of fractured surface of the *HETB*

Fig.2(a) illustrates the TEM analysis of *HETB*. Using the fast Fourier transform (FFT) of HRTEM in **fig.2(b & c), t**he d-spacing of two yellow circled regions are computed to be 4.3Å and 3.48Å, which correspond to [220] and [320] diffraction planes, as estimated from XRD data. Nb, Na, K, Ba, Sr, O are further detected by TEM-EDS analysis and found to be homogeneously distributed across the *HETB* matrix.

Materials Horizons Accepted Manuscript

View Article Online
DOI: 10.1039/D2MH01488B

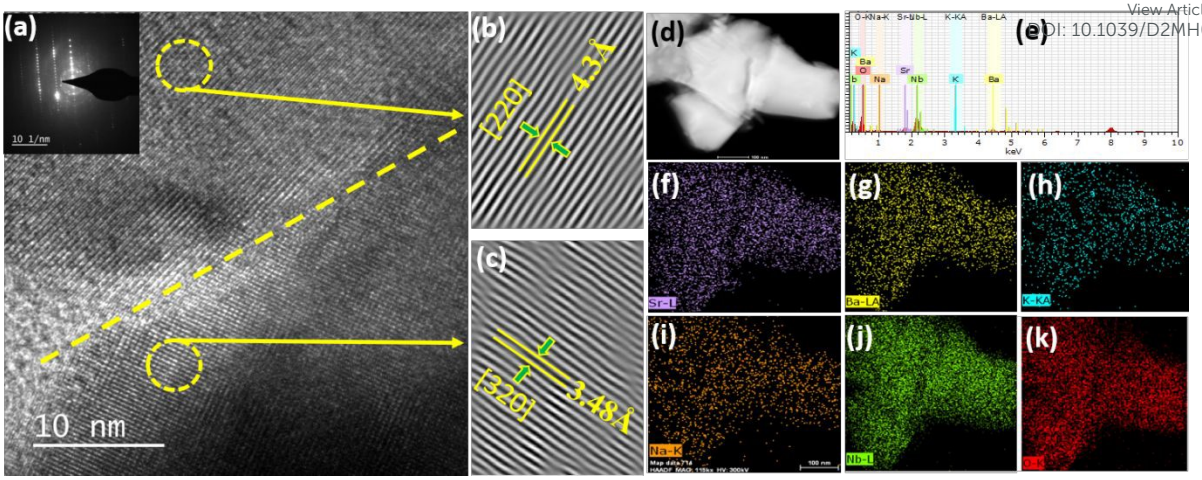

Fig.2 (a) HRTEM analysis (b) & (c) FFT of [320] and [220] planes (d) HAADF (e-k) TEM-EDS mapping.

X-ray photoelectron spectroscopy (XPS) in **fig.3(a & b)** reveals that the majority of the Nb remains in the $+5$ state and around 35% of Nb has converted into the $+4$ state due to high temperature processing of ceramics in reducing atmosphere. Colonization of lower valency metal ions (Li, Na, K) at A-site requires the formation of oxygen vacancies to maintain the charge neutrality in a single phase $(Sr_{0.2}Ba_{0.2}Li_{0.2}K_{0.2}Na_{0.2})Nb_2O_6$. Application of a reducing atmosphere facilitates the easy generation of oxygen vacancies, as evident from the deconvolution of O 1S peak. Deconvolution of the high-resolution the O 1S peak yields three distinct sub-peaks, OI (typically lattice oxygen) at $529.3eV$, OII (oxygen deficient sites) at $531.2eV$, OIII (oxygen containing groups adsorbed to the surface) at $532eV$. These values are in well agreement with literature values.[8,9,24,25] OII corresponds to the oxygen vacancy, which is found around 12% in *HETB*. This oxygen vacancy further acts as a source of electrons, participating in electron transport. Oxidation state and binding energies of Nb and O are listed in **table S4**.

Published on 28 February 2023. Downloaded by Indian Institute of Technology Kanpur on 3/7/2023 11:08:22 AM.

Materials Horizons Accepted Manuscript

View Article Online
DOI: 10.1039/D2MH01488B

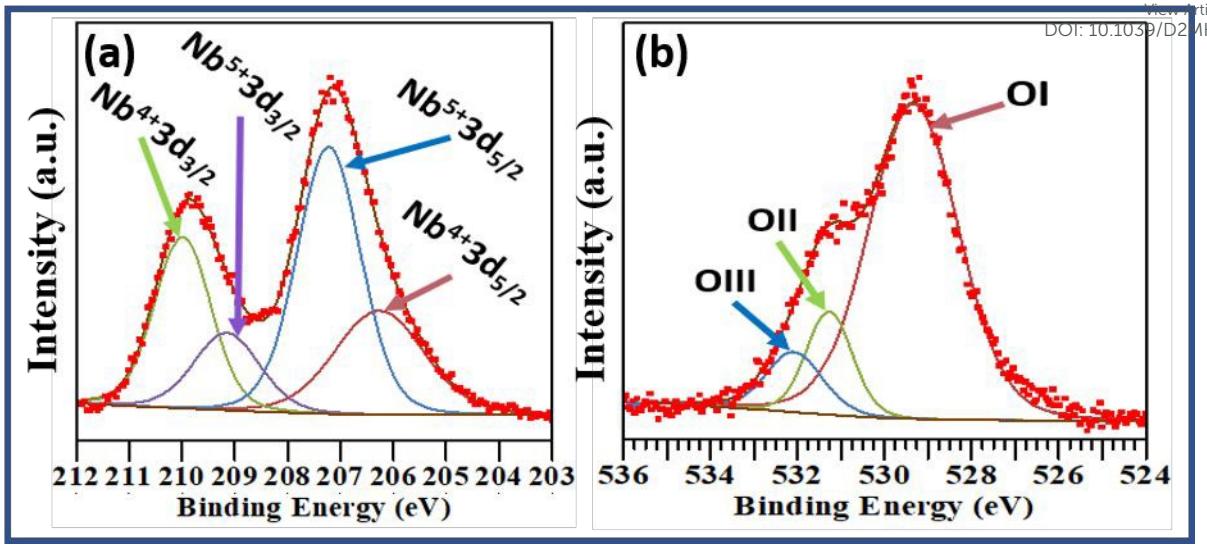

Fig.3 XPS of (a) Niobium and (b) Oxygen in HETB

Electrical transport:

The Seebeck coefficient (S) and electrical conductivity (σ), as shown in **fig.4(a & b)**, have been measured from $470K$ to $1150K$. The Seebeck coefficient is found to be negative and grows linearly (from $-270\mu VK^{-1}$at $470K$ to $-370\mu VK^{-1}$ at $1150K$) with temperature, indicating metallic or n-type degenerate semiconductor-like behavior. The Seebeck coefficient of a degenerate semiconductor can be expressed with the help of the Pisarenko relation, as shown in equation (10).[26]

$$S = \frac{8\pi^2 k_B^2}{3eh^2} m^* T \left(\frac{\pi}{3n}\right)^{2/3} \quad \text{.....(10)}$$

The maximum Seebeck coefficient has been found to be $-370\mu VK^{-1}$ at $1150K$. To the best of our knowledge, it is the highest Seebeck coefficient so far achieved for bulk SBN based tungsten bronze structures. This large Seebeck coefficient is possibly caused by the strong electron scattering in multivalent metal ions. In contrast, electrical conductivity has been found to be increasing with increase in temperature, suggesting semiconductor like behavior ($^{d\sigma}/_{dT} > 0$). The maximum electrical conductivity of $2.4 \times 10^3 Sm^{-1}$ has been obtained at $1150K$.

Published on 28 February 2023. Downloaded by Indian Institute of Technology Kanpur on 3/7/2023 11:08:22 AM.

Materials Horizons Accepted Manuscript

View Article Online
DOI: 10.1039/D2MH01488B

This synergistic rise in Seebeck coefficient and electrical conductivity with temperature allows the *HETB* to attain a maximum power factor (PF) of $324\mu Wm^{-1}K^{-2}$ at $1150K$, as shown in **fig 4(c)**.

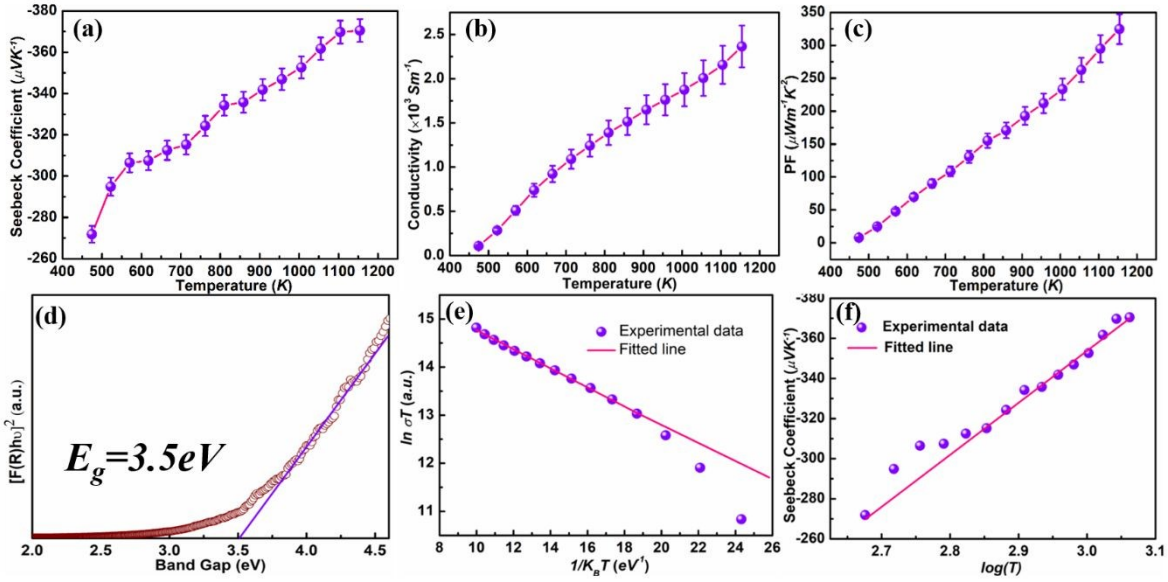

Fig.4 (a) Seebeck coefficient (b) electrical conductivity (c) power factor of *HETB* as a function of temperature (d) Plot of Kubelka-Munk function $F(R_\infty)$ vs. energy (eV) of incident radiation (e) small polaron hopping model (ln(σT) vs. $^{1}/_{K_BT}$) (f) relation of S with log (T) of *HETB*.

To better understand the charge transport of *HETB*, the band gap (E_g) has been determined using UV spectroscopy, as shown in **fig.4(d)**. Kubelka-Munk function ($F(R_\infty)$) as shown in equation (11), has been used to compute the band gap.

$$F(R_\infty) = (1 - R_\infty)^2/(2R_\infty) \ldots\ldots (11)$$

Where, the diffused reflectance (R_∞) is measured using UV-visible spectroscopy. E_g of *HETB* has been found to be $\sim 3.5eV$, which remains in the range of other tungsten bronze structures.[27–30] In fact, band gap is expected to remain almost unaffected by the multivalent cations in the A site as the valance band maxima and conduction band minima are primarily formed by the hybridization of O 2p and Nb 4d bands. Due to this large band gap, the electrical conductivity is so low that it is undetectable in the regions near room temperature. However, electrical

Published on 28 February 2023. Downloaded by Indian Institute of Technology Kanpur on 3/7/2023 11:08:22 AM.

Materials Horizons Accepted Manuscript

View Article Online
DOI: 10.1039/D2MH01488B

conductivity gradually increases with temperature, demonstrating on the order of $10^3 Sm^{-1}$ above $650K$. Nevertheless, anomalies are found in its temperature dependent Seebeck coefficient (metallic) and electrical conductivity (semiconducting), which suggest that the band model may not be adequate to explain the charge transport mechanism in *HETB*.

Further, electron concentration has been estimated using a modified Heikes' formula as mentioned in equation (12).[31–33]

$$n = \frac{A_s}{V}\left[\frac{2}{1 + e^{(S \times e)/k_B}}\right] \ldots.(12)$$

A_s is number of available sites for carriers per unit-cell and V is unit-cell volume. $(e)/k_B$ factor is approximately $0.0116\ K\mu V^{-1}$. Considering A_s equal to 5 for tungsten bronze structure and Seebeck coefficient at $450K$ we have obtained electron concentration, $n = 7 \times 10^{21} cm^{-3}$ and corresponding electron mobility ($\mu = \sigma/n.e$) has been estimated to be $0.001\ cm^2V^{-1}S^{-1}$. Using the Pisarenko relation (equation (10)), the effective mass of electrons has been estimated to be $9m_0$. Carrier concentration on the order of $10^{21}\ cm^{-3}$is considerably higher than the critical value for many thermoelectric semiconductors to undergo a semiconductor to metal transition, depicted as the Mott transition.[34–38] Surprisingly, *HETB* in our case, exhibits semiconductor-like behavior ($d\sigma/dT > 0$) in the entire temperature range, although Seebeck coefficient shows metallic behavior. The most possible explanation for the semiconductor like electrical conductivity ($d\sigma/dT > 0$) in spite of possessing such a large electron concentration is Anderson localization[39–41] of electrons, as commonly observed in many complex disordered oxides.[1,12,38,42–50] The low electron mobility and high effective mass do reflect the electron localization. The presence of multivalent metal ions, oxygen vacancies, and other atomic disorder cause variation in the local electric field, which eventually leads to electron

Published on 28 February 2023. Downloaded by Indian Institute of Technology Kanpur on 3/7/2023 11:08:22 AM.

Materials Horizons Accepted Manuscript

View Article Online
DOI: 10.1039/D2MH01488B

Published on 28 February 2023. Downloaded by Indian Institute of Technology Kanpur on 3/7/2023 11:08:22 AM.

localization at the bottom of the conduction band. Moreover, it has previously been demonstrated that nano-polarized regions in SBN based structures also act as localization centers, resulting in Anderson localization.[12,45,47,49] However, during electron conduction, electrons from one localized site require certain activation energy to delocalize or to move to the next nearest defect sites. This electron transport occurs through a thermally activated process. In such case, small polaron hopping (SPH) model[51] as expressed in equation (13) can be most appropriate to illustrate this thermally activated electron transport mechanism.

$$\sigma = \frac{\sigma_0}{T} exp^{\left(-\frac{E_{Hop}}{K_B T}\right)} \quad \text{.....(13)}$$

Small polaron hopping (SPH) model has previously been reported in many complex oxides.[45,47,52] The activation energy for hopping, E_{Hop} has been determined to be $0.198eV$ from the linear fitting of ln (σT) with $\frac{1}{K_B T}$, as shown in **fig.4(e)**.

The linear dependence of the Seebeck coefficient with temperature for *HETB*, where Anderson localization prevails, can be further explained by the Mott and cutler model[53] where S can be expressed in equation (14).

$$S = {}^{1}/_{3}\pi^2 \frac{K_B}{e}\left(K_B T \frac{dln(\mu_0)}{dE} - \frac{dE_{Hop}}{dE}\right)|_{E_F} \quad \text{.....(14)}$$

According to the Mott and cutler model, when fermi energy of a material is surrounded by a finite number of localized states and mobility edge situates above E_F, thermopower is observed to have a linear temperature dependence. However, this model is only valid in low temperature regions. Interestingly, we have observed linear dependence of S with log (T) in **fig.4(f)** at high temperatures (above 600K), which confirms the presence of localized states surrounding E_F. This behavior supports our hypothesis of Anderson localization in *HETB*. As the temperature increases, electrons from localized states are promoted above the mobility edge and participate

Materials Horizons Accepted Manuscript

View Article Online
DOI: 10.1039/D2MH01488B

in conduction, which corroborates well with the monotonically increase in σ with temperature, resulting in ~23 times enhancement in σ values.

Thermal transport:

The total thermal conductivity, as shown in **fig.5(a)** has been estimated from the experimentally measured specific heat (C_p), thermal diffusivity (D) and bulk density ρ as shown **fig.S2(a & b)** in SI. The minimum thermal conductivity has been found to be about 0.8 $Wm^{-1}K^{-1}$ at $470K$, which monotonously increases with temperature. The total thermal conductivity comprises of electronic (κ_e) and lattice (κ_l) contributions. The κ_e has been calculated using Wiedemann-Franz Law[54] ($\kappa_e = L\sigma T$). $L(W\Omega K^{-2})$ is Lorenz number and determined from the equation (15) (**fig.S2(c)**).[55]

$$L = 1.5 + \exp\left[-\frac{|S|}{116}\right] \text{.....(15)}$$

κ_e, as shown in **fig.S2(d)** is expectedly found an exact replica of electrical conductivity. However, the κ_e values obtained for *HETB* contributes less than 2% of the total κ, inferring that the overall κ is dominated by the κ_l. Lattice contribution of thermal conductivity (κ_l) is further computed by subtracting κ_e from κ, as shown in **fig.5(b)**. We have obtained minimum κ_l of 0.8 $Wm^{-1}K^{-1}$ at $470K$, which is much lower than the SBN based system.[12,15,16,47] However, it is interesting to observe that κ_l increases slightly with temperature. This abnormal κ_l behavior with temperature indicating typical glass-like behavior, has been previously reported in many SBN based oxides[12,15,47,56,57] and other complex oxides[58–60] with large point defects and large lattice distortion. Besides, this slight increment in κ_l is also possible in SBN based system due to the weakening of the domain walls,[12] which results in the steady decline in phonon scattering centers. Further, we have estimated the minimum theoretical limit (κ_{min}) of lattice thermal conductivity using Cahil's formula in equation (16).[18]

Published on 28 February 2023. Downloaded by Indian Institute of Technology Kanpur on 3/7/2023 11:08:22 AM.

Materials Horizons Accepted Manuscript

View Article Online
DOI: 10.1039/D2MH01488B

$$\kappa_{min} = \frac{K_B}{2.48} n^{\frac{2}{3}} (2v_t + v_l) \text{.....(16)}$$

Where, v_t and v_l are transverse and longitudinal velocity, as estimated from nano-indentation measurement in SI and n is number density of atom per unit volume. The κ_{min} has been found to be $0.7\ Wm^{-1}K^{-1}$, as shown by the dotted line in **fig.5(b)**. The lowest κ_l value obtained in *HETB* has been found to be very close to the κ_{min} of *HETB,* suggesting phonon glass behavior

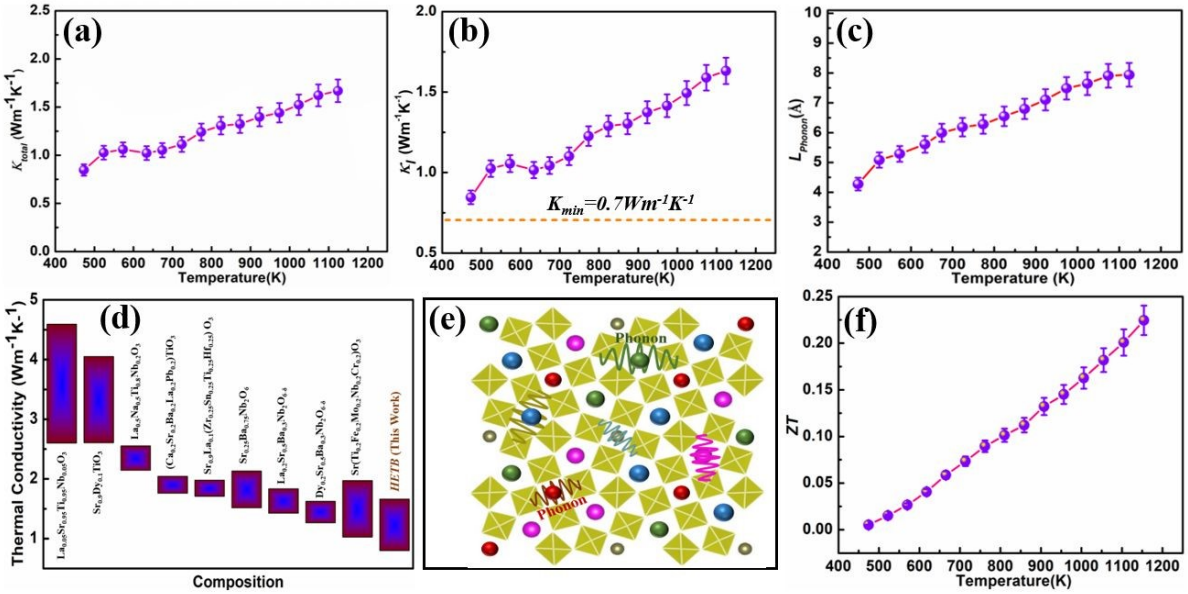

Fig.5: (a)Total thermal conductivity (b) lattice thermal conductivity with dotted line depicting minimum theoretical limit (c) mean free path of phonon with temperature (d) thermal conductivity of various thermoelectric oxides including *HETB*.[3,8,10,12,14,16,61] (e) Schematics of phonon scattering (f) variation of figure of merit (ZT) with temperature for *HETB*

Furthermore, average mean free path of phonon (L_{phonon}) has been calculated using the equation (17) and shown in **fig.5(c)**.

$$L_{phonon} = \frac{3\kappa_l}{C_v.\upsilon_m} \text{.....(17)}$$

$C_v.\upsilon_m$ are isochoric heat capacity and mean velocity of sound, respectively. The minimum L_{phonon} has been estimated to be 4.27Å at $470K$ and ranges up to 7.93Å at elevated temperatures. This remarkably low value of L_{phonon} suggests that phonon scattering occurs in the order of interatomic spacing. Authors have previously reported that the high entropy effect can induce

Published on 28 February 2023. Downloaded by Indian Institute of Technology Kanpur on 3/7/2023 11:08:22 AM.

Materials Horizons Accepted Manuscript

View Article Online
DOI: 10.1039/D2MH01488B

multi-phonon scattering, which can eventually result in ultralow lattice thermal conductivity in high entropy perovskite oxide.[3] We have achieved even lower lattice thermal conductivity in *HETB* than in HEP, which is so far the lowest among rare-earth-free high entropy oxide thermoelectrics. The thermal conductivity of various reported oxides, including *HETB,* has been presented in **fig.5(d)**. The presence of 5 multivalent metal ions is expected to induce the multi-phonon scattering by further increasing the structural complexity of inherently complex tungsten bronze structure, which helps to attain such low κ_l. A schematic of the multi-phonon scattering in the *HETB* has been shown in **fig.5(e)**, depicting the occurrence of various phonon wave lengths arising from multiple cations in the complex oxide.

Finally, ZT (**fig.5(f)**) has been calculated, and the maximum ZT has been obtained as 0.23 at $1150K$, which is about 15% larger than that of ZT value obtained in the SBN system.[12] To the best of our knowledge, this is the highest ZT value so far achieved for rare earth free high entropy oxide thermoelectrics. The rare combination of metallic Seebeck coefficient and semiconducting electrical conductivity, accompanied by extremely low thermal conductivity, allows the *HETB* to attain this excellent performance. However, high entropy engineering provides us a lot of room for further improvement in thermoelectric performance through compositional modification in numerous ways.

Conclusions:

In summary, we have successfully synthesized single phase tungsten bronze type novel high entropy $(SrBaLiKNa)_{0.2}Nb_2O_6$ ceramics. Phase analysis and microstructure study have been performed using XRD, FESEM, XPS and TEM. The lattice parameters have been determined using Rietveld refinement of powder XRD data. TEM-EDS shows the homogeneous distribution of all elements. We have obtained the maximum Seebeck coefficient of $-370\mu V K^{-1}$ at $1150K$, which is the largest Seebeck value so far obtained in SBN based bulk ceramics.

Published on 28 February 2023. Downloaded by Indian Institute of Technology Kanpur on 3/7/2023 11:08:22 AM.

Materials Horizons Accepted Manuscript

View Article Online
DOI: 10.1039/D2MH01488B

The electrical transport has been explained using small polaron hopping model. The rare combination of metal-like Seebeck coefficient and semiconductor-like electrical conductivity synergistically augurs *HETB* to attain a large power factor. In addition, the minimum thermal conductivity has been found as $0.8\ Wm^{-1}K^{-1}$ at $470K$, which is very close to the minimum theoretical limit. This ultra-low thermal conductivity combined with the excellent Seebeck coefficient allows *HETB* to attain maximum ZT of 0.23, which is so far the highest among rare earth free high entropy oxides. Although the *ZT* value has to be substantially enhanced for commercial application, this work holds great promise for the development of next generation advanced thermoelectric materials.

Acknowledgement:

This work is supported by the grant from Science and Engineering Research Board, DST (SERB-DST), India (Grant No: IMP/2018/000955).

Reference:

1 M. Acharya, S. S. Jana, M. Ranjan and T. Maiti, *Nano Energy*, 2021, **84**, 105905.
2 G. Tan, L.-D. Zhao and M. G. Kanatzidis, *Chemical reviews*, 2016, **116**, 12123–12149.
3 R. Banerjee, S. Chatterjee, M. Ranjan, T. Bhattacharya, S. Mukherjee, S. S. Jana, A. Dwivedi and T. Maiti, *ACS Sustainable Chemistry & Engineering*, 2020, **8**, 17022–17032.
4 C. M. Rost, E. Sachet, T. Borman, A. Moballegh, E. C. Dickey, D. Hou, J. L. Jones, S. Curtarolo and J.-P. Maria, *Nature communications*, 2015, **6**, 1–8.
5 M. Francis, A. Kuruvilla and L. M, *Materials Chemistry and Physics*, 2022, **292**, 126845.
6 M. Posfai and P. R. Buseck, *American Mineralogist*, 1994, **79**, 308–315.
7 R. Liu, H. Chen, K. Zhao, Y. Qin, B. Jiang, T. Zhang, G. Sha, X. Shi, C. Uher, W. Zhang and L. Chen, *Advanced Materials*, 2017, **29**, 1702712.
8 Z. Lou, P. Zhang, J. Zhu, L. Gong, J. Xu, Q. Chen, M. J. Reece, H. Yan and F. Gao, *Journal of the European Ceramic Society*, 2022, **42**, 3480–3488.
9 P. Zhang, L. Gong, Z. Lou, J. Xu, S. Cao, J. Zhu, H. Yan and F. Gao, *Journal of Alloys and Compounds*, 2022, **898**, 162858.
10 P. Zhang, Z. Lou, M. Qin, J. Xu, J. Zhu, Z. Shi, Q. Chen, M. J. Reece, H. Yan and F. Gao, *Journal of Materials Science & Technology*, 2022, **97**, 182–189.
11 S. Lee, R. H. Wilke, S. Trolier-McKinstry, S. Zhang and C. A. Randall, *Applied Physics Letters*, 2010, **96**, 031910.
12 Y. Li, J. Liu, Y. Hou, Y. Zhang, Y. Zhou, W. Su, Y. Zhu, J. Li and C. Wang, *Scripta Materialia*, 2015, **109**, 80–83.
13 M. Ohtaki, K. Araki and K. Yamamoto, *Journal of Electronic Materials*, 2009, **38**, 1234–1238.
14 J. Wang, B.-Y. Zhang, H.-J. Kang, Y. Li, X. Yaer, J.-F. Li, Q. Tan, S. Zhang, G.-H. Fan, C.-Y. Liu, L. Miao, D. Nan, T.-M. Wang and L.-D. Zhao, *Nano Energy*, 2017, **35**, 387–395.

Published on 28 February 2023. Downloaded by Indian Institute of Technology Kanpur on 3/7/2023 11:08:22 AM.

Materials Horizons Accepted Manuscript

View Article Online
DOI: 10.1039/D2MH01488B

15 Y. Li, J. Liu, Y. Zhang, Y. Chen, J. Li, W. Su, H. Wang and C. Wang, *Ceramics International*, 2017, **43**, 13345–13348.
16 Y. Li, J. Liu, Y. Zhang, Y. Chen, J. Li, W. Su, H. Wang, J. Zhai, T. Wang and C. Wang, *Journal of the European Ceramic Society*, 2017, **37**, 3039–3043.
17 J. H. Chan, J. A. Bock, H. Guo, S. Trolier-McKinstry and C. A. Randall, *Journal of Materials Research*, 2017, **32**, 1160–1167.
18 D. G. Cahill, S. K. Watson and R. O. Pohl, *Physical Review B*, 1992, **46**, 6131.
19 P. B. Jamieson, S. C. Abrahams and J. L. Bernstein, *The Journal of Chemical Physics*, 1968, **48**, 5048–5057.
20 L. A. Bursill and P. J. Lin, *Acta Crystallographica Section B: Structural Science*, 1987, **43**, 49–56.
21 T. Woike, V. Petříček, M. Dušek, N. K. Hansen, P. Fertey, C. Lecomte, A. Arakcheeva, G. Chapuis, M. Imlau and R. Pankrath, *Acta Cryst B*, 2003, **59**, 28–35.
22 S. Aronson, Estimation of the heat of formation of refractory mixed oxides, *Journal of Nuclear Materials* 107(2/3) (1982) 343-346 .
23 R. F. Zhang, S. H. Zhang, Z. J. He, J. Jing and S. H. Sheng, *Computer Physics Communications*, 2016, **209**, 58–69.
24 J. Bao, X. Zhang, B. Fan, J. Zhang, M. Zhou, W. Yang, X. Hu, H. Wang, B. Pan and Y. Xie, *Angewandte Chemie*, 2015, **127**, 7507–7512.
25 B. Wang, J. Yao, J. Wang and A. Chang, *Journal of Alloys and Compounds*, 2022, **897**, 163188.
26 N. ASHCROFT and N. MERMIN, *New York*.
27 C. Sun, X. Guo, C. Hu, L. Liu, L. Fang, Z. Cheng and N. Luo, *RSC Advances*, 2021, **11**, 13386–13395.
28 D. Fan, R. Chong, F. Fan, X. Wang, C. Li and Z. Feng, *Chinese Journal of Catalysis*, 2016, **37**, 1257–1262.
29 M. Zhang and X. Zuo, *Journal of Alloys and Compounds*, 2019, **806**, 386–392.
30 J. Ruiz-Fuertes, O. Gomis, A. Segura, M. Bettinelli, M. Burianek and M. Mühlberg, *Applied Physics Letters*, 2018, **112**, 042901.
31 H. Taguchi, M. Sonoda and M. Nagao, *Journal of Solid State Chemistry*, 1998, **137**, 82–86.
32 D. Srivastava, C. Norman, F. Azough, M. C. Schäfer, E. Guilmeau, D. Kepaptsoglou, Q. M. Ramasse, G. Nicotra and R. Freer, *Physical Chemistry Chemical Physics*, 2016, **18**, 26475–26486.
33 D. Srivastava, C. Norman, F. Azough, D. Ekren, K. Chen, M. J. Reece, I. A. Kinloch and R. Freer, *Journal of Materials Chemistry A*, 2019, **7**, 24602–24613.
34 L. Bjaalie, A. Janotti, B. Himmetoglu and C. G. Van de Walle, *Physical Review B*, 2014, **90**, 195117.
35 T. Okuda, K. Nakanishi, S. Miyasaka and Y. Tokura, *Phys. Rev. B*, 2001, **63**, 113104.
36 W. Wunderlich, H. Ohta and K. Koumoto, *Physica B: Condensed Matter*, 2009, **404**, 2202–2212.
37 C. Lee, J. Destry and J. L. Brebner, *Physical Review B*, 1975, **11**, 2299.
38 P. Dey, S. S. Jana, F. Anjum, T. Bhattacharya and T. Maiti, *Applied Materials Today*, 2020, **21**, 100869.
39 P. W. Anderson, *Physical review*, 1958, **109**, 1492.
40 P. Bernasconi, I. Biaggio, M. Zgonik and P. Günter, *Phys. Rev. Lett.*, 1997, **78**, 106–109.
41 H. Ihrig and D. Hennings, *Phys. Rev. B*, 1978, **17**, 4593–4599.
42 P. Roy, V. Waghmare and T. Maiti, *RSC Advances*, 2016, **6**, 54636–54643.
43 Sudha, M. Saxena, K. Balani and T. Maiti, *Materials Science and Engineering: B*, 2019, **244**, 65–71.
44 M. Saxena and T. Maiti, *Journal of Alloys and Compounds*, 2017, **710**, 472–478.
45 J. A. Bock, S. Trolier-McKinstry, G. D. Mahan and C. A. Randall, *Physical Review B*, 2014, **90**, 115106.

Published on 28 February 2023. Downloaded by Indian Institute of Technology Kanpur on 3/7/2023 11:08:22 AM.

Materials Horizons Accepted Manuscript

View Article Online
DOI: 10.1039/D2MH01488B

46 S. Lee, G. Yang, R. H. Wilke, S. Trolier-McKinstry and C. A. Randall, *Physical Review B*, 2009, **79**, 134110.
47 Y. Li, J. Liu, Y. Zhang, Y. Zhou, J. Li, W. Su, J. Zhai, H. Wang and C. Wang, *Ceramics International*, 2016, **42**, 1128–1132.
48 S. S. Jana and T. Maiti, *ACS Applied Materials & Interfaces*, 2022, **14**, 14174–14181.
49 Y. Li, J. Liu, C.-L. Wang, W.-B. Su, Y.-H. Zhu, J.-C. Li and L.-M. Mei, *Chinese Physics B*, 2015, **24**, 047201.
50 S. S. Jana and T. Maiti, *Carbon*, , DOI:10.1016/j.carbon.2022.11.039.
51 I. G. Austin and N. F. Mott, *Advances in Physics*, 1969, **18**, 41–102.
52 M. Schrade, R. Kabir, S. Li, T. Norby and T. G. Finstad, *Journal of Applied Physics*, 2014, **115**, 103705.
53 M. Cutler and N. F. Mott, *Phys. Rev.*, 1969, **181**, 1336–1340.
54 C. Kittel, *Introduction to solid state physics*, Wiley, Hoboken, NJ, 8th ed., 2005.
55 H.-S. Kim, Z. M. Gibbs, Y. Tang, H. Wang and G. J. Snyder, *APL Materials*, 2015, **3**, 041506.
56 E. Fischer, W. Haessler and E. Hegenbarth, *Physica Status Solidi A, Applied Research*, 1982, **72**, K169–K171.
57 T. Kolodiazhnyi, H. Sakurai, O. Vasylkiv, H. Borodianska and Y. Mozharivskyj, *Applied Physics Letters*, 2014, **104**, 111903.
58 L. Chen, Y. Jiang, X. Chong and J. Feng, *Journal of the American Ceramic Society*, 2018, **101**, 1266–1278.
59 J. Yang, X. Qian, W. Pan, R. Yang, Z. Li, Y. Han, M. Zhao, M. Huang and C. Wan, *Advanced Materials*, 2019, **31**, 1808222.
60 J. He, G. He, P. Wang, L. Xu, J. Liu and J. Tao, *J Mater Sci*, 2022, **57**, 17563–17576.
61 L. M. Daniels, S. N. Savvin, M. J. Pitcher, M. S. Dyer, J. B. Claridge, S. Ling, B. Slater, F. Cora, J. Alaria and M. J. Rosseinsky, *Energy & Environmental Science*, 2017, **10**, 1917–1922.

Published on 28 February 2023. Downloaded by Indian Institute of Technology Kanpur on 3/7/2023 11:08:22 AM.

Materials Horizons Accepted Manuscript